ISSN 1070-3284, Russian Journal of Coordination Chemistry, 2022, Vol. 48, No. 8, pp. 516–525. © Pleiades Publishing, Ltd., 2022.

The issue is dedicated to the 70th birthday of Academician V.I. Ovcharenko

Synthesis, Crystal Structure, Hirshfeld Surface Analysis and DFT Calculations of Two New Cu(II) and Cd(II) Complexes with the 4-Amino-6-methoxypyrimidine Ligand

S. Sahli[a], F. Lefebvre[b], C. Jelsch[c], C. Ben Nasr[a], and K. Kaabi[a, *]

[a] *Laboratoire de Chimie des Matériaux, Université de Carthage, Faculté des Sciences de Bizerte, Zarzouna, 7021 Tunisia*

[b] *Laboratoire de Chimie Organométallique de Surface (LCOMS), Ecole Supérieure de Chimie Physique Electronique, Villeurbanne Cedex, 69626 France*

[c] *CRM2, CNRS, Institut Jean Barriol, Université de Lorraine, Vandoeuvre les Nancy Cedex, France*

**e-mail: kamel_kaabi@yahoo.fr*

Received October 15, 2021; revised December 15, 2021; accepted December 23, 2021

Abstract—Two new mononuclear complexes, $[Cu_2Cl_{1.23}(NO_3)_{0.77}(Ampy)_4(H_2O)_4](NO_3)_2{\cdot}4H_2O$ (**I**) and $[CdI_2(Ampy)_2]$ (**II**) (Ampy = 4-amino-6-methoxypyrimidine) have been synthesized and characterized by single crystal X-ray diffraction studies (CCDC nos. 2023331 (**I**), 2023331 (**II**)) at 295 K for (**I**) and 100 K for (**II**). The structure of the Cu(II) complex shows that the Cu(II) central atom is five-coordinated with a distorted square pyramidal geometry. In compound (**II**) the Cd(II) cations are tetracoordinated with a distorted tetrahedral fashion. Intermolecular interactions were investigated by Hirshfeld surfaces. Electronic properties such as HOMO and LUMO energies were derived.

Keywords: Cd(II) complex, Cu(II) complex, X-ray diffraction, coordination compound, Hirshfeld surface, DFT calculations

DOI: 10.1134/S1070328422080061

INTRODUCTION

Pyrimidines are ideal as ligands for the formation of coordination complexes with virtually any type of metal cation due to their two nitrogen atoms of the pyrimidine ring which react as two donor centers and the ability of these nitrogen atoms to form hydrogen bonds that play an essential role for the structural stability of these complexes. Moreover, the presence of two nitrogen atoms allows the formation of a bridge between two metal atoms, thus making possible the formation not only of coordination polymers [1], but also binuclear polymers bridged by pyrimidine [2]. Among metal complexes, the copper complexes show interesting chemical and physical properties significant for catalysis, gas storage, luminescence, fluorescence and magnetism [3–6]. As well, the coordination chemistry of cadmium has received significant interest due to the increased recognition of its role in biological systems and structural chemistry [7, 8]. Furthermore, d^{10} electronic configuration and zero crystal field stabilization energy facilitate Cd(II) ions to adopt various geometries including tetrahedron, trigonal bipyramidal, square pyramidal, octahedral and dodecahedron [9]. The structural diversity of metal complexes depends essentially on the nature of the metal atom, the ligand and the counterion. In this respect, we used mixed-salt $Cu(NO_3)_2$ and $CuCl_2$ to synthesize a new complex $[Cu_2Cl_{1.23}(NO_3)_{0.77}(Ampy)_4(H_2O)_4](NO_3)_2{\cdot}4H_2O$ (**I**) with Ampy (4-amino-6-methoxypyrimidine) as organic ligand and two inorganic ligands (NO_3^- and Cl^-) in order to provide a structure different from that of the complex $[Cu(Ampy)(H_2O)(NO_3)_2]$ [10]. We have also synthesized another new metal complex $[CdI_2(Ampy)_2]$ (**II**) with a metal atom Cd(II) and Ampy as organic ligand. These complexes were studied by various physicochemical methods including DFT studies, single crystal X-ray diffraction and Hirshfeld surface analysis. The Hirshfeld surface analysis was performed to completely characterize the intermolecular interactions and explain the crystalline architecture.

EXPERIMENTAL

In the paper, the following compounds were used: Ampy (purity 96%, Sigma-Aldrich), $Cu(NO_3)_2{\cdot}3H_2O$

Table 1. Crystallographic data and refinement details of the complexes **I** and **II**

Parameter	Value	
	I	**II**
Crystal data		
Chemical formula	$C_{20}H_{44}N_{14.77}O_{20.33}Cl_{1.23}Cu_2$	$C_{10}H_{14}N_6O_2I_2Cd$
M_r	987.26	616.47
Crystal system, space group	Monoclinic, $C2/c$	Monoclinic, $P2_1/n$
Temperature, K	295	100
a, Å	16.4258(4)	7.299(2)
b, Å	13.5316(3)	15.340(3)
c, Å	18.9009(6)	16.223(3)
β, deg	106.830(3)	102.40(3)
V, Å^3	4021.11(19)	1773.9(7)
Z	4	4
μ, mm^{-1}	1.23	4.72
Crystal size, mm	0.19 × 0.17 × 0.17	0.09 × 0.08 × 0.07
T_{min}, T_{max}	0.896, 1.130	0.507, 0.579
Reflections collected/unique	10178/4669	39444/4060
R_{int}	0.025	0.126
$\sin\theta_{max}/\lambda$, Å^{-1}	0.687	0.650
Independent parameters	319	192
$R(F^2 > 2\sigma(F^2))$, $wR(F^2)$, S	0.038, 0.103, 1.04	0.053, 0.091, 1.16
$\Delta\rho_{max}/\Delta\rho_{min}$, e Å^{-3}	0.37/−0.29	1.32/−1.16

(purity 98%, Sigma-Aldrich), $CuCl_2{\cdot}2H_2O$ (purity 99%, Sigma-Aldrich), and CdI_2 (purity 99%, Sigma-Aldrich).

Synthesis of complex (I). A solution of Ampy (0.6 mmol) in ethanol (10 mL) was added to an aqueous solution (10 mL) of a mixture of $Cu(NO_3)_2{\cdot}3H_2O$ (0.28 mmol), and $CuCl_2{\cdot}2H_2O$ (0.13 mmol). The mixture was then stirred for 1 h at room temperature. The resulting solution was filtered and the filtrate was kept at room temperature for slow evaporation. After 9 days, blue crystals were obtained (the yield was 62%).

For $C_{20}H_{44}N_{14.77}O_{20.33}Cl_{1.23}Cu_2$ (**I**)

Anal. calcd., %	C, 24.31	H, 4.46	N, 20.94
Found, %	C, 24.49	H, 4.63	N, 20.78

Synthesis of complex II. A solution of Ampy (0.4) in ethanol (10 mL) was added to a solution of CdI_2 (0.2 mmol) in water (10 mL). After stirring for 45 min, the mixture was filtered and the resultant solution was allowed to evaporate at room temperature. Transparent prismatic single crystals of the complex **II**, which remained stable under normal conditions of temperature and humidity, were isolated after several days and subjected to X-ray diffraction analysis (the yield was 61%).

For $C_{10}H_{14}N_6O_2I_2Cd$ (**II**)

Anal. calcd., %	C, 19.46	H, 2.26	N, 15.90
Found, %	C, 19.15	H, 2.57	N, 15.69

X-ray structure determination. Diffraction data were collected at 293 K on a New Xcalibur EosS2 single crystal diffractometer with graphite monochromated MoK_α radiation (λ = 0.71073 Å). Unit cell determination, data collection and data reduction were performed using the CrysAlisPro software [11]. A symmetry-related (multiscan) absorption correction has been applied. The structure was solved with ShelXT [12] and refined by a full-matrix least-squares procedure based on F^2 using the ShelXL-2014 [13, 14]. Crystallographic data of the complexes are sum-

marized in Table 1. The drawings were made with Diamond [15] and Mercury [16].

Diffraction data of compound **II** were obtained at 100 K on a Bruker D8 Venture diffractometer equipped with a Photon III CMOS area detector and with a MoK_α radiation ($\lambda = 0.71073$ Å) X-ray microfocus source. The X-ray intensities were corrected using multi-scan method applied by SADABS [17]. The crystal structure was solved by use of the ShelXT program using intrinsic phasing method and refined by full-matrix least-square techniques on F^2 using the ShelXL-2014 program [12–14]. All non-hydrogen atoms were refined as anisotropic. The positions of all hydrogen atoms were introduced at ideal position and refined as riding atoms with isotropic displacement parameters ADPs ($U_{iso}H = 1.2U_{eq}C_{Arom}$, $1.2U_{eq}N$ and $1.5U_{eq}C_{Meth}$). The crystal data are gathered in Table 1. The drawings were made with Diamond [15] and Mercury [16].

Theoretical calculations. As our aim was to study the compounds in the solid state the positions of all atoms, except hydrogens, were those determined by X-ray study. The positions of hydrogen atoms, introduced at their ideal positions in the X-ray study, were optimized before the calculation of the properties of the compound. So no full optimization was made, only the positions of hydrogens are not those given by the X-ray study. Note that quite the same modification of H positions was made for Hirschfeld analysis.

RESULTS AND DISCUSSION

The main geometrical features of the different chemical entities of **I** are given in Table 2. X-ray crystal structure analysis reveals that the compound crystallizes in the monoclinic space group *C*2/*c*. Figure 1a represents the Ortep view of the asymmetric unit of the Cu(II) complex with all atoms occupying a general position in the complex and it shows that the asymmetric unit consists of a Cu(II) cation, two 4-amino-6-methoxylpyrimidine ligands, two coordinated water molecules, 0.61 occupancy coordinated Cl^- anion, 0.39 coordinated NO_3^- anion, one uncoordinated NO_3^- anion and two co-crystallized water molecules with the hydrogen atom of the water molecule $O(12)H_2$ disordered on two positions H(12A) and H(12C) with an 0.5/0.5 occupancy rate of. In the atomic arrangement, the central atom Cu(II) is pentacoordinated in a square pyramidal geometry, on the other hand, the same central atom of the complex [Cu(Ampy)$(H_2O)(NO_3)_2$] [10] is hexacoordinated in an octahedral geometry. Due to the disorder, there are two types of square pyramid coordination of the central Cu(II) atom, CuO_2N_2Cl or CuO_3N_2. The apical position of the first pyramid is occupied by a chloride anion, while in the second pyramid it is occupied by the O(9) atom of the $N(3)O_3^-$ nitrato ligand. The percentages of the two square pyramids in the structure are, respectively, 61.3 and 38.7%. Bond lengths and angles around the Cu(II) ion are given in Table 2. The basal Cu–O bond distances (Cu–O(3) 1.975(2) Å and Cu–O(4) 1.996(2) Å) are shorter than the apical Cu–O bond distance (Cu–O(9) 2.257(5) Å). This fact may be ascribed to a Jahn–Teller distortion. The Cu–N bond distances range from 2.0115(19) to 2.005(2) Å and the Cu–Cl bond distance is 2.6548(18) Å. These bond distances agree with those found in other complexes [18, 19]. The *cis*-XCuCl (X = N or O) angles in the CuO_2N_2Cl square pyramid range from 92.44(7)° to 99.91(7)°, while the XCuO(9) angles in the CuO_3N_2 square pyramid range from 80.2(2)° to 112.1(2)°. This indicates that the CuO_3N_2 square pyramid is more distorted than the CuO_2N_2Cl one. In the atomic arrangement, the square pyramid $CuO_2N_2ClO(9)$ and two co-crystallized water molecule $H_2O(11)$ and $H_2O(12)$ are interconnected *via* hydrogen bonds of the O–H...O and O–H...Cl types to give a 1D corrugated chain running along the $[10\bar{1}]$ direction (Fig. 1b). These chains are arranged so that the Cu(II) cations are located parallel to the *b, c* plane at $x = n \pm 1/4$ and the organic ligands are located between them. The chemical entities existing in this structure are linked together by 27 hydrogen bonds to form a three-dimensional network (Fig. 1c). These hydrogen bonds are divided into four types: O–H...O, O–H...Cl, N–H...O and N–H...Cl. The crystal packing is also stabilized by aromatic stacking interactions between the pyrimidine rings with an interplanar distance of 3.834 Å (Fig. 1).

The main geometrical features of the different chemical entities of the [CdI_2(Ampy)$_2$] coordination compound are reported in Table 3. X-ray crystal structure analysis reveals that the coordination compound crystallizes in the monoclinic space group $P2_1/n$. The asymmetric unit of the title compound consists of one Cd(II) cation, two 4-amino-6-methoxylpyrimidine organic ligands and two iodine ions (Fig. 2a). The Cd(II) atom is coordinated by two pyrimidine nitrogen atoms (N(1A) and N(1B) of the two 2-amino-4-methylpyrimidine ligands, and two iodine atoms (I(1) and I(2)) to form a CdI_2N_2 polyhedron with a slightly deformed tetrahedral geometry. The detailed geometry of the CdI_2N_2 tetrahedron (Table 3) shows that the bond distances are the following: Cd–N(1A) 2.252(6), Cd–N(1B) 2.242(7), Cd–I(1) 2.7561(12) and Cd–I(2) 2.7451(12) Å. This geometry is comparable to that observed in the bis{μ-1-[(2-ethyl-1*H*-imidazol-1-yl)meth-yl]-1*H*-benzotria-zole}bis(iodidocadmium) complex of formula [$Cd_2I_4(C_{12}H_{13}N_5)_2$] [20] where the average values of Cd–N and Cd–I bond lengths are 2.276 and 2.6993 Å, respectively. The bond angles around the Cd atom of the title compound vary between 102.8(2)° and 118.97(17)°, a similar range of values was observed in the [$Cd_2I_4(C_{12}H_{13}N_5)_2$] com-

Table 2. Selected bond distances (Å) and angles (deg) for complexes **I**

Bond	*d,* Å	Bond	*d,* Å
N(1)–Cu	2.0115(19)	O(4)–Cu	1.996(2)
N(4)–Cu	2.005(2)	O(9)–Cu	2.257(5)
O(3)–Cu	1.975(2)	C(11)–Cu	2.6548(18)
Angle	ω, deg	Angle	ω, deg
O(3)CuC(11)	92.44(7)	O(3)CuN(1)	92.14(8)
O(4)CuC(11)	99.91(7)	O(4)CuN(1)	86.65(8)
N(4)CuC(11)	97.46(7)	N(4)CuN(1)	169.62(8)
N(1)CuC(11)	92.61(6)	O(3)CuO(9)	112.1(2)
O(3)CuO(4)	167.63(9)	O(4)CuO(9)	80.2(2)
O(3)CuN(4)	89.94(8)	N(4)CuO(9)	92.11(17)
O(4)CuN(4)	89.15(8)	N(1)CuO(9)	96.52(16)

Table 3. Comparison between selected bond distances and angles in $[CdI_2(Ampy)_2]$ and complex $[Cd_2I_4(C_{12}H_{13}N_5)_2]$ [29]

$[CdI_2(Ampy)_2]$		$[Cd_2I_4(C_{12}H_{13}N_5)_2]$ [29]	
Bond	*d,* Å	Bond	*d,* Å
Cd(1)–I(2)	2.7451(12)	Cd(1)–I(1)	2.7094(4)
Cd(1)–I(1)	2.7561(12)	Cd(1)–I(2)	2.6892(4)
Cd(1)–N(1B)	2.242(7)	Cd(1)–N(1)	2.302(3)
Cd(1)–N(1A)	2.252(6)	Cd(1)–N(5)^{i}	2.250(3)
Angle	ω, deg	Angle	ω, deg
I(2)Cd(1)I(1)	106.46(3)	I(2)Cd(1)I(1)	118.809(14)
N(1B)Cd(1)I(2)	106.31(17)	N(1)Cd(1)I(1)	109.18(8)
N(1B)Cd(1)I(1)	118.97(17)	N(1)Cd(1)I(2)	108.30(8)
N(1B)Cd(1)N(1A)	102.8(2)	N(5^{i})Cd(1)N(1)	99.31(11)
N(1A)Cd(1)I(2)	116.45(19)	N(5^{i})Cd(1)I(1)	106.59(8)
N(1A)Cd(1)I(1)	106.43(19)	N(5^{i})Cd(1)I(2)	112.86(8)

plex with angles between 99.31(11) and 118.809(14)° (Table 3). In the structural arrangement, the amino group and the pyrimidine nitrogen of neighboring molecules are linked together through two pairs of N(3A)–H...N(2A) and N(3B)–H...N(2B) hydrogen bonds to form a 1D corrugated chain running along the [011] direction (Fig. 2b). The CdI_2Cl_2 tetrahedra are located parallel to the *a, c* plane at $y = n \pm 1/4$ between the organic molecules (Fig. 2c).

The Hirshfeld surface is representative of the region in space where molecules come into contact with each other allowing the analysis of the chemical nature of intermolecular interactions in the crystal. The contact enrichment ratio is obtained by comparing the actual contacts C_{XY} in the crystal with those computed as if all types of contacts had the same probability to form. An enrichment ratio larger than unity for a given pair of chemical species X...Y indicates that these contacts are over-represented in the crystal [21]. The analysis of contact types and their enrichment were computed with the program MoProViewer [22]. The two independent organic molecules show very different contacts and Fingerprint plots (Figs. 3a, 3b). Therefore, the Hirshfeld surface was computed around each organic molecule present in the crystal (two organic entities) in order to analyze the crystal contacts (Figs. 3c, 3d). The Cu...O coordination bond represents, by far, the most enriched contact in both compounds with $E_{CuO} = 4.8$ and 5.3, respectively, followed by the Cu...N coordination bond ($E_{CuO} = 4.6$ and 5.1). The Cu cation is coordinated by two water oxygen atoms, two nitrogen atoms, one oxygen nitrate or one chloride anion. The most abundant contacts between the organic molecules are constituted by H...H contacts ($C_{HH} = 21$ and 24%) (Figs. 3a, 3b). The O...Hn contacts between the oxygen nitrate, water

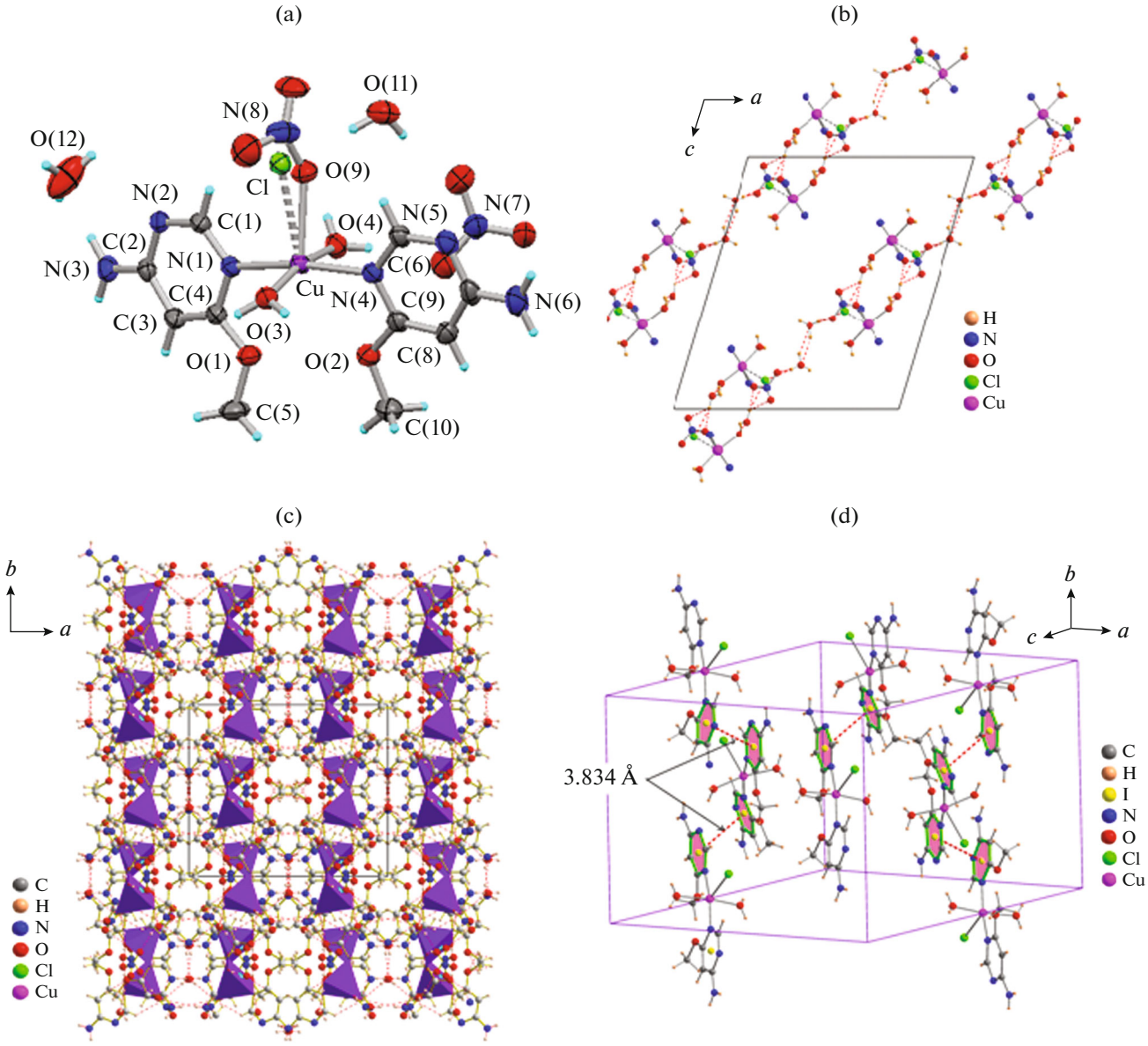

Fig. 1. ORTEP of the structure of **I** (a), view of the 1D chain $\{[Cu_2Cl_{1.23}(NO_3)_{0.77}(H_2O)_4]\cdot 4H_2O\}_n$ along *c* axis (b), projection of the structure of **I** along the *c* axis (c) and stacking interactions between neighboring aromatic rings in **I** (d).

oxygen and organic cations, are over-represented at $E_{OH_n} = 1.69$ and 1.9 around the first and second molecule, respectively. The H_n...N hydrogen bonds amounts are 4.4 and 4.0% of the Hirshfeld surface and these contacts are over-represented with enrichments equal to 1.33 and 1.18 for the two organic molecules. The fingerprint plots of the organic molecules show a N...H spike at short distance only for molecule #1 (Figs. 3a, 3b). Moreover, concerning O...H/H...O strong H-bonds, there is only a H...O spike at short distance for molecule #1. The fingerprint plots present also a short contact spike for the N...Cu coordination contact. Besides, the C_4N_2 aromatic cycle of the organic molecule forms antiparallel stacking with itself, resulting in quite enriched C...C interactions with $E_{cc} = 2.5$ and 1.94, respectively, for the two organic molecules [23]. Hydrophobic contacts (between Hc and C) are over-represented with $E = 1.12$ in molecule #1 but are under-represented with $E = 0.64$ in molecule #2 and represent 2.8 and 4.2%, respectively, on the Hirshfeld contact surface of the organic entities. The chloride anions are almost exclusively surrounded by hydrogen atoms. The Hn...Cl contacts are absent in the first molecule but very enriched with $E = 2.85$ in the second organic entity and are referred to the strong N–H...Cl^- hydrogen bonds. The interactions between the charged Cl^- and hydrophobic Hc atoms are over-represented with $E =$

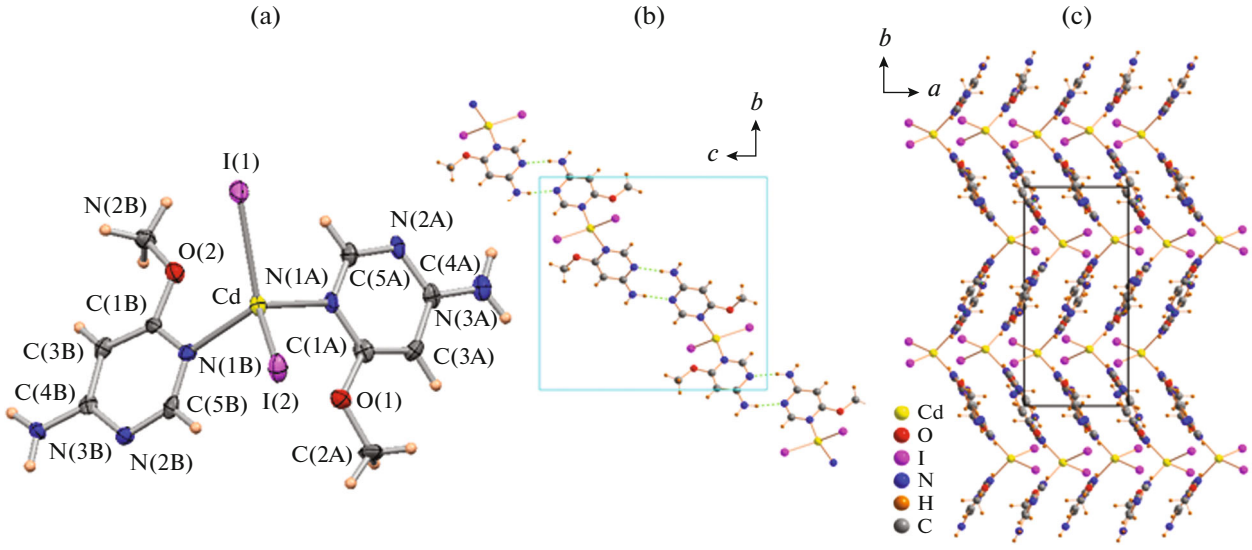

Fig. 2. ORTEP of the structure of **II** (a), view of 1D zigzag chain $[CdI_2(Ampy)_2]_n$ along the [011] direction (b) and crystal packing arrangement viewed along *c* axis (c) (dotted lines indicate hydrogen bonds).

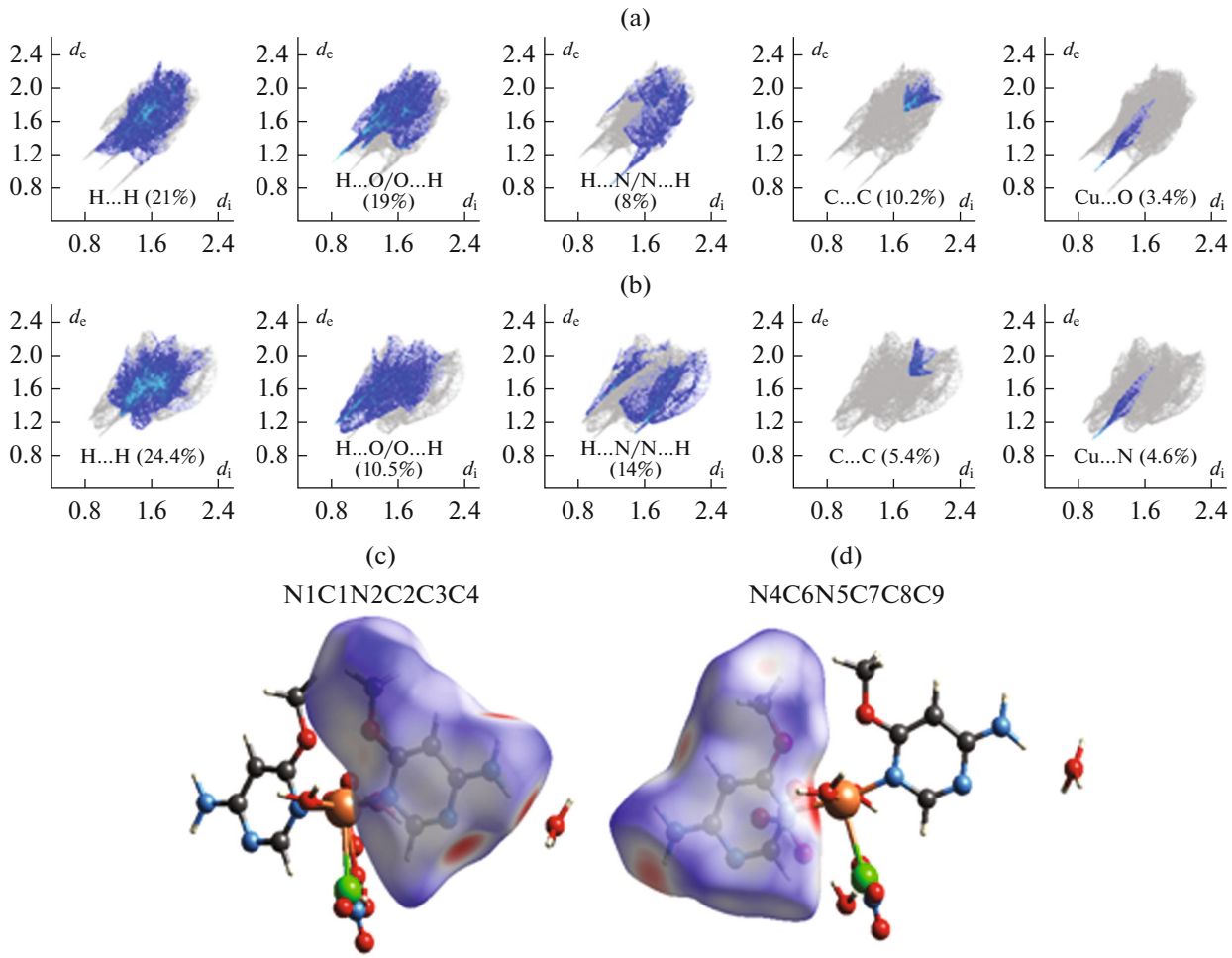

Fig. 3. 2D fingerprint (d_i, d_e) plots of the Hirshfeld surface around the first molecule in compound **I** (a), fingerprint (d_i, d_e) plots of the Hirshfeld surface around the second molecule (b), Hirshfeld surface around the first organic molecule in **I** (c), Hirshfeld surface around the second organic molecule (d). (For interpretation of the references to color in this figure legend, the reader is referred to the web version of this article).

Table 4. Statistical analysis of intermolecular contacts on the Hirshfeld surface in compound **II**. The second row shows the chemical content on the Hirshfeld surface. C_{XY} represents the actual contact types and E_{XY} their enrichment ratios. Reciprocal contacts (X···Y and Y···X) are merged. The main contacts and the most enriched ones are highlighted in bold

Atom	Cd	I	H_n	N	O	H_c	C
% surface	8.7	28.0	9.7	10.9	4.0	23.4	15.4
Cd	0.0	**10.2**	0.9	6.6	2.7	1.3	1.2
I		3.6	**5.6**	1.2	2.1	**23.6**	**8.2**
Hn			0.8	**6.3**	0	1.0	3.1
N				1.0	0	1.2	3.8
O					0	1.2	0.4
Hc						6.1	4.1
C							4.0
Cd	0.00	**1.55**	0.43	**2.72**	**3.49**	0.25	0.34
I		0.42	1.05	0.20	1.11	**1.82**	0.98
Hn			0.90	**3.28**	0	0.24	1.17
N				0.86	0	0.26	1.27
O					0	0.86	0.46
Hc						1.24	0.64
C							**1.94**

2.56 in molecule #1 and 1.25 in molecule #2, and can be considered as weak C(I).

The contacts made by the two ligands A and B in compound **II** are almost indistinguishable and the fingerprint plots shown in Fig. 4a correspond to the ensemble of two ligands. The two molecules are related by a pseudo-twofold axis along the *a* direction. The actual contact surfaces C_{XY} show a high correlation $r = 98.1\%$. The two iodine atoms are also related by this pseudo-symmetry and their coordinates $x \approx 0.4$ are similar. The contact types C_{XY} of the two iodine atoms are 93% correlated. The H···H contacts are the largest contribution (35.7%) to the total Hirshfeld surface of the ligand in the fingerprint plots. The second most abundant interaction is N...H (16.3%) and the strong hydrogen bond N–H...N are responsible for the two spikes at short distances (d_e, d_i). A third spike is due to N...Cd coordination. A spike at larger d_e distance is due to the H...I contacts, mostly weak C–H...I hydrogen bonds. The O...H contacts occur at distance *d*(H...O) larger than 2.8 Å and are C–H...O hydrogen bonds between a weak donor (methyl hydrogen) and a weak acceptor (ether oxygen). Aromatic stacking interactions yield mostly C...C and C...N contacts. The intermolecular interactions of the asymmetric unit content (Fig. 4b) were evaluated by computing the contacts enrichment ratios (*E*, Table 4) in order to highlight which contacts are over-represented. The enriched contacts are likely to represent energetically attractive interactions and the driving force in crystal formation. The non-polar atoms C and H_c constitute less than 40% of the Hirshfeld surface and the stacking contacts C...C are significantly enriched ($E = 1.94$). The contacts with largest surface are the weak H-bonds I...Hc and the coordination Cd...I which are both over-represented (enrichment larger than one). The cadmium cation is mostly surrounded by the negatively charged atoms: iodide, nitrogen and oxygen and all these contacts are enriched.

Quantum chemical calculations were performed from the crystal data with the DFT method at the B3LYP/6-31+G* level, using the Gaussian 09 program. The HOMO and LUMO molecular orbitals of **I** were determined in the first case for the complex with the chloride ion and in the second case for the complex with the nitrate ion (Figs. 5a, 5b). In both cases, the HOMO is localized essentially on the inorganic ion chloride or nitrate, while the LUMO is mainly located on the organic ligands. The energy gap between HOMO and LUMO is 4.89 eV for the complex with chlorine and 3.92 eV for the complex with nitrate which is therefore a little less stable. These values imply high kinetics stability and low chemical reactivity for compound **I** [24, 25].

The HOMO and LUMO orbitals of complex **II** were also determined (Fig. 5c). A system including the cadmium atom, the two organic ligands, and the two

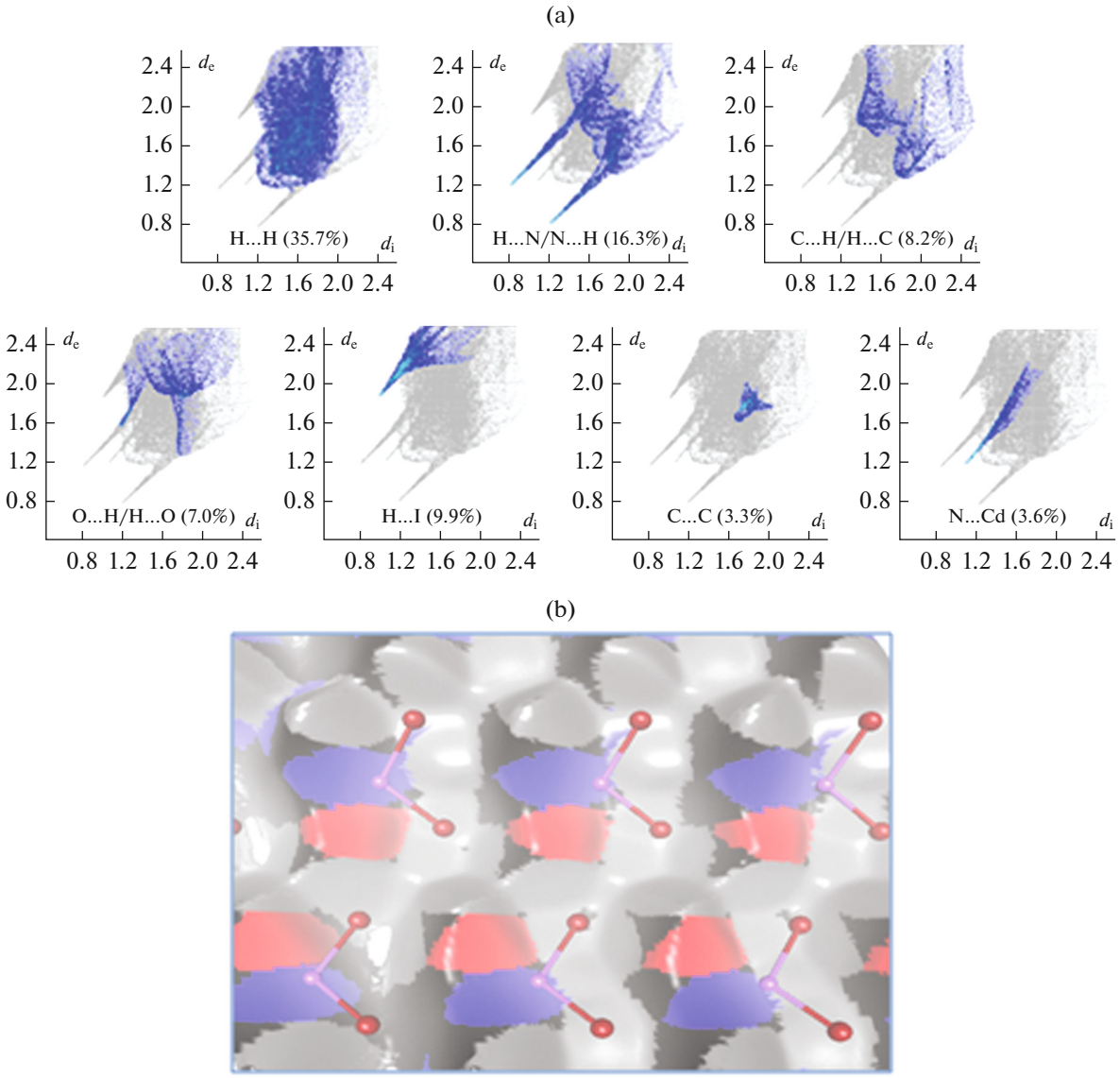

Fig. 4. Hirshfeld surface fingerprint plots of the contacts around the 2-amino-6-methoxypyrimidine ligand B in **II** (a), autostereogram view of the Hirshfeld surface between the CdI_2 and ligand layers around the plane $y = 1/4$ in compound **II** (b) (the CdI_2 moieties are shown in ball and stick above the surface. Unit cell vector **a** is horizontal; grey: hydrogen, black: carbon, blue: nitrogen, red: oxygen, brown: iodine, purple: cadmium).

iodine ions was studied by use of the B3LYP/6-31+G* method. Clearly, the highest occupied orbital (HOMO) is mainly localized on the two iodine ions bounded to the cadmium atom, while the lowest unoccupied orbital (LUMO) is localized on one of the organic ligands. The large HOMO–LUMO energy gap of 3.67 eV corresponds also to high stability.

The Molecular electrostatic potential (MEP) surface of compound **I**, depicted in Figs. 5d, 5e, is used to determine the nuclear and electronic charge distribution of a given molecule. The maps were obtained at the B3LYP/6-31+G* level of theory. Moreover, blue and red colours indicate the positive and negative potentials, respectively. As it can be seen, the electrostatic potential maps are color-coded and are subdivided into many regions. The negative charges are found mainly on chlorine and nitrate ion, the most positive part being towards the hydrogens of water molecules. The MEP of compound **II** is depicted in Fig. 5f. The most negative areas are on the iodine atoms as well as on the aromatic carbon bonded to the NH_2 group, while the positive zones are on the methyl groups and the protons of the NH_2 group.

In summary, two new complexes $[Cu_2Cl_{1.23}(NO_3)_{0.77}(Ampy)_4(H_2O)_4](NO_3)_2{\cdot}4H_2O$ and $[CdI_2(Ampy)_2]$ were successfully synthesized at room temperature by slow evaporation. The contact enrichment ratios, derived from the Hirshfeld surface analysis,

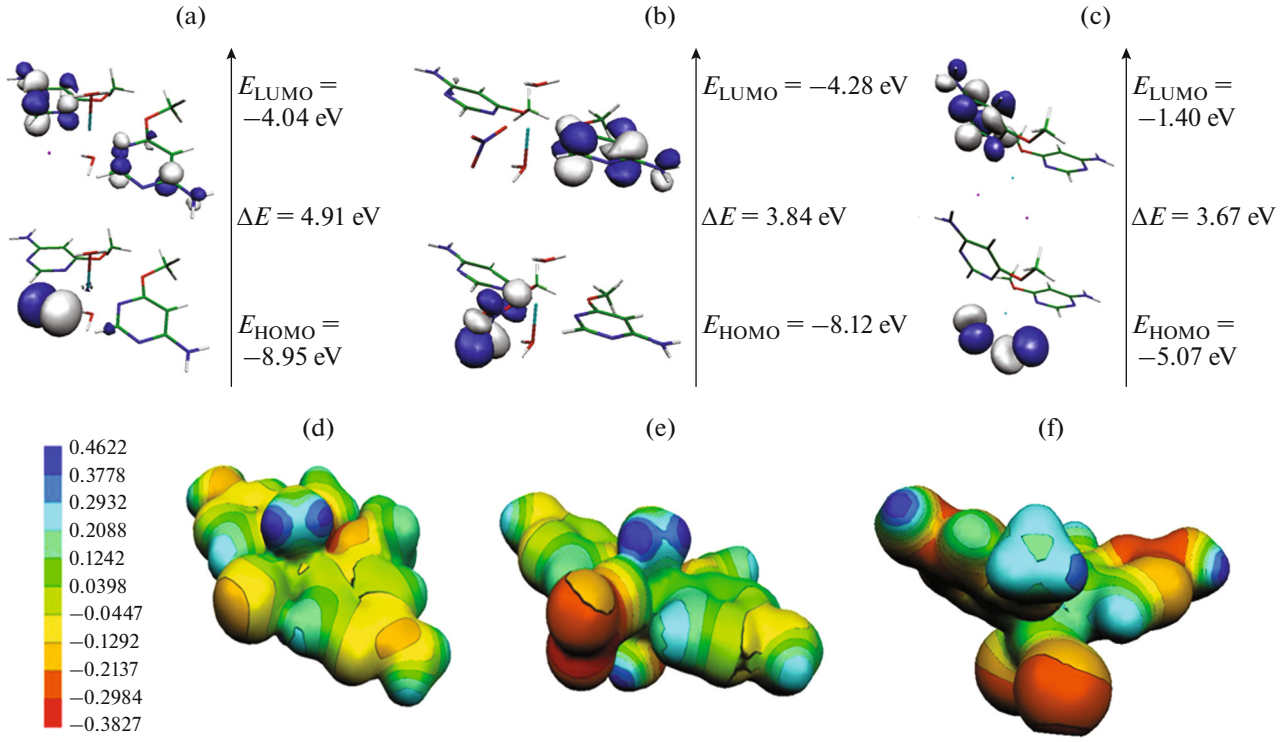

Fig. 5. Frontier orbitals in complexes: **I** with chloride ion (a), **I** with nitrate ion (b), **II** (c), MEP surface of complex **I** with chloride ion (d) or with nitrate ion (e), MEP surface of complex **II** (f).

allowed determining which types of contacts are over-represented. For compound **I**, the Cu...O and Cu...N coordination bonds represent the most enriched contacts. For the two independent organic molecules, the most abundant contacts are constituted by the Hc...Hn and Hc...Hc interactions. For compound **II**, Cd...O, Cd...N and Cd...I^- coordination interactions are dominant, these interactions are all quite over-represented. Moreover, the HOMO–LUMO energy gap suggests a good stability of these compounds. MEP analysis reveals, for compound **I** that the negative charges are found mainly on chlorine and nitrate ions, the most positive part being on the hydrogen atoms of water molecules. For compound **II**, the most electronegative areas are on the iodide anion as well as on the aromatic carbon bonded to the NH_2 group, while the positive zones are on the methyl groups and the protons of the NH_2 group.

FUNDING

The authors did not receive support from any organization for the submitted work.

CONFLICT OF INTEREST

The authors declare that they have no conflicts of interest.

REFERENCES

1. Bridgewater, B.M. and Parkin, G., *J. Am. Chem. Soc.*, 2000, vol. 122, no. 29, p. 7140.
2. Roy, S., Antonio, B., Frontera, A., and Chattopadhyay, S., *Inorg. Chim. Acta*, 2016, vol. 450, p. 321.
3. Hart, L.R., Harries, J.L., Greenland, B.W., et al., *ACS Appl. Mater. Interfaces*, 2015, vol. 7, p. 8906.
4. Pan, L., Olson, D.H., and Ciemnolonski, L.R., *Angew. Chem., Int.*, 2006, vol. 45, p. 616.
5. Zhuo, H.Y., Su, H.F., Cao, Z.Z., et al., *Chemistry*, 2016, vol. 22, p. 17619.
6. McQuade, L.E. and Lippard, S.J., *Inorg. Chem.*, 2010, vol. 49, p. 7464.
7. Pal, P.K., Mohapatra, S., Jana, A.D., and Patra, G.K., *J. Mol. Struct.*, 2012, vol. 1015, p. 156.
8. Näther, C., Wöhlert, S., Boechmann, J., Wriedt, M.I., and Jeß, Z., *Anorg. Allg. Chem.*, 2013, vol. 639, no. 15, p. 2696.
9. Rochon, F.D. and Fakhfakh, M., *Inorg. Cmim. Acta.*, 2009, vol. 362, p. 1455.
10. Nbili, W., Kaabi, K., Ferenc, W., et al., *J. Mol. Struct.*, 2017, vol. 1130, p. 114.
11. *CrysAlisPro, Agilent Technologies, Version 1.171.37.35 (release 13-08-2014) CrysAlis171.NET*, compiled August 13, 2014,18:06:01; CrysAlisPro 1.171.38.41, Rigaku OD, 2015.
12. Sheldrick, G.M., *Acta Crystallogr., Sect. A: Found. Crystallogr.*, 2008, vol. 64, p. 112.

13. Sheldrick, G.M., *SHELXL-97*, Göttingen: Univ. of Göttingen, 1997.
14. Sheldrick, G.M., *Acta Crystallogr., Sect. C: Struct. Chem.*, 2015, vol. 71, p. 3.
15. Brandenburg, K., *Diamond, version 2.0*, Bonn: Impact GbR, 1998.
16. Macrae, F., Bruno, I.J., Chisholm, J.A., et al., *J. Appl. Cryst.*, 2008, vol. 41, p. 466.
17. *SADABS, Version 2016/2*, Madison: Bruker AXS Inc., 2016.
18. Vynohradov, O.S., Pavlenko, V.A., Safyanova, I.S., et al., *Acta Crystallogr., Sect. E: Crystallogr. Commun.*, 2020, vol. 76, p. 1507.
19. Molano, M.F., Velasquez, V.P.L., Erben, M.F., et al., *Acta Crystallogr., Sect. E: Crystallogr. Commun.*, 2020, vol. 76, p. 148.
20. Xia, W. and Jun, N., *Acta Crystallogr., Sect. E: Struct. Rep. Online*, 2011, vol. 67 p, p. 882.
21. Jelsch, C., Ejsmont, C., and Huder, L., *IUCrJ*, 2014, vol. 1, p. 119.
22. Guillot, B., Enrique, E., Huder, L., and Jelsch, C., *Acta Crystallogr., Sect. A: Found. Adv.*, 2014, vol. 70, p. 279.
23. Jelsch, C., Soudani, S., and Ben Nasr, C., *IUCrJ*, 2015, vol. 2, p. 327.
24. Saikat, K.S., Seth, B., and Tanusree, K., *J. Mol. Struct.*, 2010, vol. 965, p. 45.
25. Saikat, K.S., Nitish, C.S., Soumen, G., and Tanusree, K., *Chem. Phys. Lett.*, 2011, vol. 506, no. 4, p. 309.